Defect-induced strong electron-phonon interaction and localization in $Sr_2FeMo_{1-x}W_xO_6$ ($x=0.0, 0.2, 0.5, 0.8, 1.0$)

Néstor E. Massa*
Laboratorio Nacional de Investigación y Servicios en Espectroscopía Óptica-Centro CEQUINOR, Universidad Nacional de La Plata, C.C. 962, 1900 La Plata, Argentina

José Antonio Alonso, María Jesús Martínez-Lope, and María Teresa Casais
Instituto de Ciencia de Materiales de Madrid, Consejo Superior de Investigaciones Científicas, Cantoblanco, E-28049 Madrid, Spain
(Received 6 October 2004; revised manuscript received 9 August 2005; published 12 December 2005)

We report on infrared reflectivity and transmission spectra of Sr_2FeMoO_6 samples with ~70% of Fe/Mo cationic ordering. In addition to an overdamped Drude component, localized secondary features are assigned to itinerant carriers interacting strongly with infrared active longitudinal optical modes of quasipolar insulating patches. Their origin is traced to antisite imperfections, and particularly, to antiphase boundary interactions. This implies that carriers are always prone to localization beyond the oxides standard scenario recreating electron localization and small polaron conductivity. Our finding is also supported by a remarkable well-defined second order spectra. The comparison between two samples of Sr_2FeMoO_6 with ~70% and ~92% of Fe/Mo cationic ordering shows that by reducing the number the defects, there is an increment in the phonon coherent length yielding a cleaner picture in the most perfectly ordered sample. In $Sr_2FeMo_{1-x}W_xO_6$ solid solutions that scenario is maintained up to $x \leqslant 0.5$ where breathing modes of Fe, Mo, and W octahedra sustain the strongest electron-phonon interaction. The reflectivity of $Sr_2FeMo_{0.2}W_{0.8}O_6$ has well-defined phonon bands, a residual Drude contribution, and a distinctive low temperature small polaron localization. We also found that Sr_2FeWO_6 is an insulator structurally stable from 20 to 700 K with a gap about 750 cm^{-1} (~95 meV). We conclude that the main clue for understanding low-field magnetoresistance resides in those interacting carriers, their confinement, and the important polaronic effects.

DOI: 10.1103/PhysRevB.72.214303 PACS number(s): 71.38.−k, 63.50.+x, 78.30.−j, 71.27.+a

I. INTRODUCTION

It has been long recognized that the understanding of two intimate items such as defects and low-field magnetoresistance may yield potential applications for oxides in the development of magnetic devices. Among those, double perovskites are good candidates for these endeavors since they have been found to be magnetoresistive at room temperature.

$A_2BB'O_6$ double perovskites attracted the interest of many as early as the 1960s.[1–3] In particular, Sr_2FeMoO_6 has been recognized as one outstanding spin polarized system with carriers giving, according to several band calculations, a half-metal character due to a minority down-spin finite density of states at the Fermi level. The down-spin conduction band crossing E_F is dominated by Fe $3d$–Mo $4dt_{2g\downarrow}$ states while the up-spin band below E_F is mostly due to the Fe $3de_{g\uparrow}$.[4–6] Measurements confirmed that the Fe $e_{g\uparrow}$ and the Fe+Mo$t_{2g\downarrow}$ band are distributed from −2.2 to −0.9 eV and from −0.9 eV to E_F, respectively.[7,4]

With decreasing temperature, Sr_2FeMoO_6 undergoes a gradual change from a metallic state into a paramagnetic insulating state at about 550 K. At 410 K, there is also a structural phase transition from cubic $Fm3m$ to tetragonal $I4/m$, below which Sr_2FeMoO_6 again becomes metallic.[8,9]

The Fe magnetic lattice is aligned ferromagnetically in the tetragonal phase and the opposite spin orientation is found for itinerant t_{2g} carriers from Mo, yielding a net ferrimagnetic character for this phase. dc susceptibility measurements indicate strong coupling in Fe and Mo sites between those localized Fe cores and the delocalized itinerant electrons. Presumably, t_{2g} electrons are allowed to hop from site to site only if the Fe core spins are oriented antiparallel to them. Thus magnetic ordering in Sr_2FeMoO_6 is realized when ferromagnetic coupling between Fe ions is mediated by the mobile electrons.[10]

Mössbauer spectroscopy showed that disorder associated with Fe, Mo[11–13] is individualized mainly as antisites point defects or antiphase boundaries leading to planes of Fe-O-Fe bonds which couple antiferromagnetically. This situation is in contrast with localized antiferromagnetism in insulating Sr_2FeWO_6.[13]

Xanes results for K and $L2,3$ edges confirmed that, in Sr_2FeMoO_6, Fe is in FeII/III mixed valence state resulting in strong mixing with Mo itinerant electrons.[14]

It is then understood that a net increase in the low-field magnetoresistance in FeMo double perovskites is linked to the alternating Fe-Mo cation order. Antisite disorder in Sr_2FeMoO_6, containing Mo atoms at the Fe position and vice versa, have been shown to have dramatic influence in the magnetic and magnetotransport properties. A comparison between ordered samples [~70% of cationic ordering, ordered moments of $3.9(1)\mu_B$ and $-0.37(6)\mu_B$ for the Fe and Mo positions] and a nominally disordered sample (~18% of cationic ordering) reveals a similarly strong neutron magnetic scattering, which is attributed to long-range antiferromagnetic correlations associated with Fe—O—Fe superexchange interactions.[8]

It is concluded that in low-field magnetoresistance, connectivity between grains does not seem to be an issue since that effect was found in samples prepared at 2 GPa as well as

with several other techniques.[15,16] Chemical inhomogeneities, associated with several (111) planes of iron, would create a more insulating environment that is expected to result in well-defined infrared active phonon bands reminiscent of those found in semiconducting compounds.[17]

The $Sr_2FeMo_{1-x}W_xO_6$ ($0 \leqslant x \leqslant 1$) series has attracted our attention. It offers an exceptional opportunity to study the localization of electrons as Mo is substituted by W, thus decreasing the number of itinerant carriers, in spite of the fact that Sr_2FeMoO_6 and Sr_2FeWO_6 are isoelectronic. Also, antisite disorder effects are thought to be minimized in this series, because the introduction of the highly charged W^{6+} cation favors the B'/B'' ordering. A structural study[18] shows that the room temperature crystal structure of the former members of the series ($x \leqslant 0.5$) is tetragonal ($I4/m$), and is characterized by a single antiphase tilt of the FeO_6 and $(Mo,W)O_6$ octahedra along the c axis; this structure evolves to the more distorted monoclinic ($P2_1/n$) for $x=0.8$ and $x=1.0$, containing three kinds of unequivalent oxygen atoms. The driving force of the structural phase transition is the promotion of the voluminous Fe^{2+} cations upon W substitution, as demonstrated by a bond valence study. The phase transition is accompanied by a sudden decrease of the distortion of the FeO_6 and $(Mo,W)O_6$ octahedra. The progressive localization of the carriers induces a smooth evolution of the volume and the lattice parameters with the W content.

This is consistent with the phase diagram proposed by Daas and Goodenough[13] for $Sr_2FeMo_{1-x}W_xO_6$ with exhibits resistivities that range from metalliclike at $x=0$ to insulatinglike for $x=1$. At intermediate concentrations, such as for $x=0.5$, semiconducting resistivity is observed at room temperature close to a metal to insulator transition.[13,19] When W is introduced, the effect is the same as for an increment in the number of Fe-O-Fe patches, in the sense that stoichiometric conducting regions are further apart.

In this paper, we present infrared reflectivity and transmission spectra of the solid solutions $Sr_2FeMo_{1-x}W_xO_6$ ($x=0.0,0.2,0.5,0.8,1.0$). We identify absorptions bands associated in SrFeO–like lattice defects, i.e., antiferromagnetic Fe-O-Fe patches, which we attribute to localized features due to itinerant carriers interacting strongly with longitudinal optical modes. We also contrast our results with those by Tomioka and co-workers in defect free Sr_2FeMoO_6 single crystals where a clear magnetoresistive effect has not yet been observed.[19,20]

II. SAMPLE PREPARATION AND CHARACTERIZATION

The series $Sr_2FeMo_{1-x}W_xO_6$ ($x=0.2,0.5,0.8,1$) was prepared by soft-chemistry procedures. Stoichiometric amounts of analytical grade $Sr(NO_3)_2$, $FeC_2O_42H_2O$, $(NH_4)_6Mo_7O_{24}4H_2O$, and $H_{26}N_6O_{41}W_{12}18H_2O$ were dissolved in citric acid. The citrat+nitrate solutions were slowly evaporated, leading to organic resins containing a homogeneous distribution of the involved cations. These resins were first dried at 120 °C and then slowly decomposed at temperatures up to 600 °C for 12 h. For the $x=0.2,0.5$ compounds, the precursors were annealed at 820 °C for 6 h in a H_2/N_2 (5%/95%) reducing flow. The $x=0.8$ sample was treated at 900 °C in a H_2/Ar (1%/99%) flow for 6 h. The term of the series, Sr_2FeWO_6, was heated in H_2/N_2 (5%/95%) at 1000 °C for 6 h. The $x=0$ compound Sr_2FeMoO_6 has been prepared as described in Ref. 16. The degree of ordering obtained from x-ray diffraction (XRD) was found to be greater than 90% in all the samples. An extra Sr_2FeMoO_6 sample with a lower degree of disorder, for comparative purposes, was prepared by annealing the corresponding precursor at 1050 °C for 12 h in a H_2-N_2 (5%/95%) flow.[18]

The degree of Fe/Mo ordering was established by Rietveld analyses of the x-ray diffraction (Cu $K\alpha$, $\lambda = 1.5406$ Å) patterns and it was also consistent with the reported measurements of the saturation magnetization. Further characterization was done by neutron diffraction patterns taken at the SLAD facility of the Studsvik Neutron Research Laboratory, Sweden (partially ordered sample, $x=0$) (Ref. 8) or the Institut Laue-Langevin ($x=0,0.2,0.5,0.8,1.0$ samples).[18] The present samples are the same previously investigated in the mentioned neutron diffraction studies.[8]

For Sr_2FeMoO_6, the structure was refined in the cubic $Fm3m$ space group above 415 K, in agreement with Chmaissen *et al.*[21] Below this temperature the crystal structure was defined in the $I4/m$ space group. For the solid solutions, the room temperature crystal structure with $x=0.2$ and $x=0.5$ was defined in the tetragonal $I4/m$ space group, and for the $x=0.8$ and $x=1$ perovskites, the monoclinic $P2_1/n$ space group was used, as indicated in the Introduction. No changes in symmetry were observed in any of the samples down to 2 K.[16,18,22]

III. Experimental and spectral analysis

Near, medium, and far infrared reflectivity and transmission spectra between 30–10 000 cm^{-1} were measured at different temperatures in a Fourier transform infrared (FT-IR) Bruker 113v interferometer with 2 cm^{-1} (far infrared and mid-infrared) and 6 cm^{-1} (near infrared) resolution. As-prepared pellets were used in reflectivity measurements using a gold mirror as 100% reference. Bulk transmission of $Sr_2FeMo_{1-x}W_xO_6$ ($x \leqslant 0.5$) microcrystals, random embedded in semitransparent CsI and polyethylene 1-cm-diameter pellets, were employed to verify reproducibility and that surface effects do not play a role in the detection of weak reflectivity features (see below).

Our samples were mounted on a cold finger of an OXFORD DN 1754 cryostat for measurements between 77 and 500 K. We also used a homemade high temperature chamber, suitable for the Bruker 113v vacuum environment, in runs from room temperature to 750 K.

We estimated phonon frequencies using a standard multioscillator dielectric simulation (Ref. 23) fit of reflectivity spectra, using the phonon frequencies obtained from their respective transmission spectra as the initial values of the frequencies.

The dielectric function $\varepsilon(\omega)$ is given by

$$\varepsilon(\omega) = \varepsilon_1(\omega) + i\varepsilon_2(\omega) = \varepsilon_\infty \prod_j \frac{(\Omega_{j\mathrm{LO}}^2 - \omega^2 + i\gamma_{j\mathrm{LO}}\omega)}{(\Omega_{j\mathrm{TO}}^2 - \omega^2 + i\gamma_{j\mathrm{TO}}\omega)}. \quad (1)$$

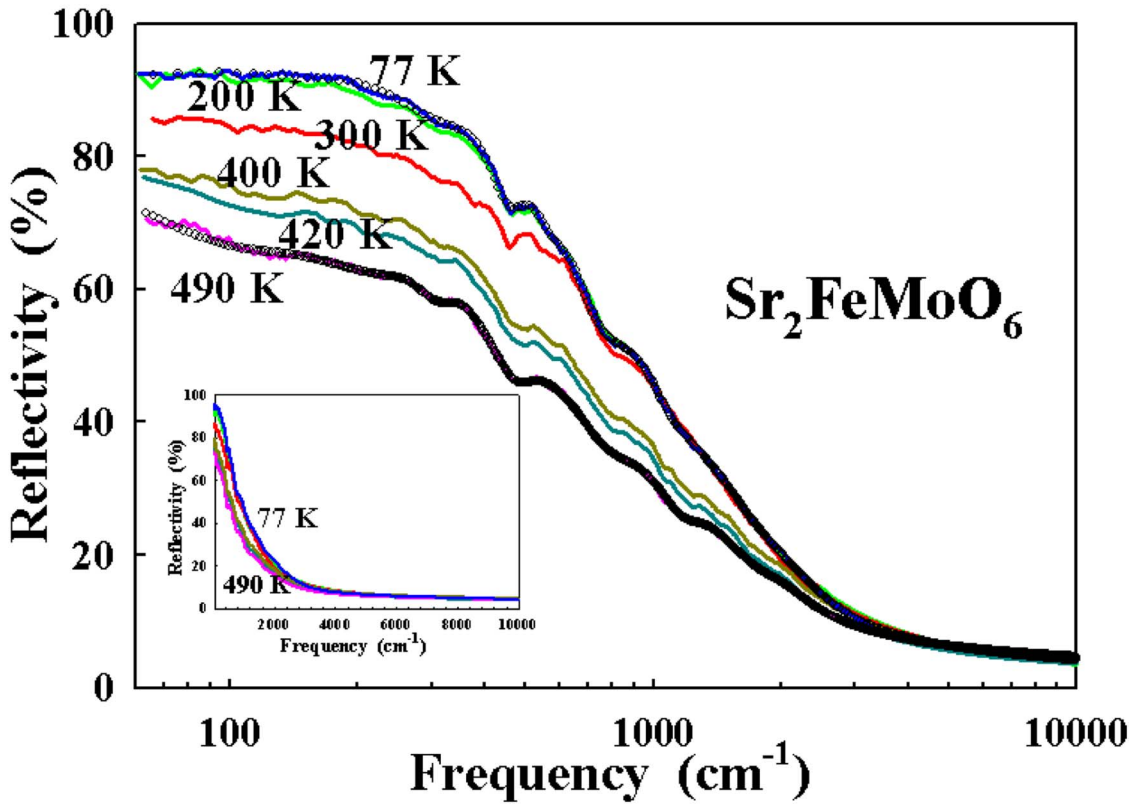

FIG. 1. (Color online) Temperature dependent reflectivity spectra of Sr_2FeMoO_6 with ~70% of cationic ordering. Full lines: experimental; open circles: fitted. Inset: The tail, a feature common to conducting oxides, is plotted in a lineal scale.

We then optimized the normal reflectivity against the experimental points and calculated the high frequency dielectric function ε_∞, the transverse and longitudinal optical frequencies $\Omega_{j\mathrm{TO}}$ and $\Omega_{j\mathrm{LO}}$, and their transverse and longitudinal damping constants $\gamma_{j\mathrm{TO}}$ and $\gamma_{j\mathrm{LO}}$, respectively. We also calculated the S_j strength of the jth oscillator as

$$S_j = \Omega_{j\mathrm{TO}}^{-2} \frac{(\prod_k \Omega_{k\mathrm{LO}}^2 - \Omega_{j\mathrm{TO}}^2)}{(\prod_{k\neq j} \Omega_{k\mathrm{TO}}^2 - \Omega_{j\mathrm{TO}}^2)}, \tag{2}$$

In addition, when the spectra required it, we added the plasma contribution (Drude term) to the dielectric simulation function as

$$-\frac{[\Omega_{\mathrm{pl}}^2 + i(\gamma_p - \gamma_0)\omega]}{[\omega(\omega - i\gamma_0)]}, \tag{3}$$

where Ω_{pl} is the plasma frequency, γ_{pl} its damping, and γ_0 is understood as a phenomenological damping introduced to reflect lattice drag effects. When these two dampings are set equal, one retrieves the classical Drude formula.[24] With

$$\Omega_{\mathrm{pl}}^2 = 4\pi e^2 N/m^*, \tag{4}$$

we estimate an effective carrier concentration $N^* = Nm_0/m^*$ (m_0 and m^* are the free- and effective electron mass; N and N^* are the number and the effective number of carriers, respectively. In our case we have used $m^* \sim 10m_0$ since it is about the value regularly found for high correlated carriers in oxides).

IV. Sr_2FeMoO_6

Figure 1 shows that the reflectivity of fresh Sr_2FeMoO_6 is similar to those already reported for conducting oxides. That is, from 77 to 490 K, it has a Drude component and a long tail that extends toward near infrared frequencies (Fig. 1, inset) associated with hopping electron conductivity, here, likely between Fe and Mo sites in the net ferrimagnetic ordering.[10] On cooling through the phase transition at ~410 K, the effective number of carriers increases, i.e., the reflectivity rises at the rate larger than the expected for conducting oxides. While changes from 300 to 77 K in metallic $LaNiO_3$ (Ref. 17), a nickelate with electron-phonon interactions not as strong as in double perovskites, is ~15%, the jump for Sr_2FeMoO_6 in the same temperature interval is ~50%. We may then speculate that by lowering the temperature we might be also optimizing the free carrier path through of a possible extra mechanism involving only T_{2g} -Mo-Fe minority electrons. The 77 K plasma edge is at ~9000 cm^{-1}(~1.1 eV) (Table I), is in agreement with values reported by Marimoto *et al.*,[25] Tomioka *et al.*,[19] and Jung *et al.*[26] However, Drude analysis, summarized Table I, yields a heavily overdamped plasma highlighting that itinerant carriers in Sr_2FeMoO_6 with antisite imperfections are always prone to localization. It also brings up a scenario common to electron localization and small polaron conductivity in oxides. The reflectivity tail that weakens asymptotically toward higher frequencies as the photon energy increases is generated in a way that the electron hops, from site to site, until it

TABLE I. Fitting parameters in the dielectric simulation for Sr_2FeMoO_6.

Temperature (K)	ε_∞	ω_{TO} (cm^{-1})	ω_{LO} (cm^{-1}) ω_p (cm^{-1})	γ_{TO} (cm^{-1}) γ_0 (cm^{-1})	γ_{LO} (cm^{-1}) γ_p (cm^{-1})	S (cm^{-2})
		80.2	85.5	704.2	592.3	2.7
		127.7	134.4	118.8	253.3	1.8
		272.6	297.3	111.3	83.7	4.4
		336.9	343.1	113.6	448.3	0.96
		378.6	457.7	1455.9	85.4	4.76
		503.1	544.0	137.1	1780.2	1.35
		555.1	505.9	1554.9	377.1	0.35
300	1.59	656.3	738	319.9	190.1	0.73
		834.6	1104.8	433.6	245.8	1.06
		1225.3	1374.7	438.4	2148.5	0.25
		1440.0	1581.5	1500.8	683.4	0.25
		1990.1	2112.0	739.3	828.6	0.11
			6907.8	8681.6	15621.3	
		79.5	82.2	233.5	1890.2	4.12
		89.3	92.4	313.5	1883.9	2.45
		120.9	125.5	392.8	127.9	3.95
		151.9	160.5	423.5	1775.8	3.59
		254.9	276.3	1350.6	220.7	7.84
		327.0	340.3	1183.6	259.7	5.4
77	1.34	362.9	451.8	257.3	118.0	7.87
		510.0	544	137.8	137.5	3.73
		550.9	611.8	451.8	1024.8	0.81
		618.1	739.4	535.5	245.7	0.30
		834.8	1105.2	1348.5	282.4	1.81
		1112.8	1374.7	393.6	496.2	0.05
		1455.9	1741.6	556.2	777.9	0.18
		1905.4	2356.0	1824.2	758.7	0.15
			9020.2	5381.3	17859.9	

finds a continuum due to multiphonon processes of different orders. The optical absorption is then dominated by polaron hops accompanied by phonon summation processes as second order phonon sum combinations of different orders; contributing because of the overlap in frequency of different orders.[27] In our case, Sr_2FeMoO_6 with ~30% of antisite disorder, anharmonicities and localization combine in a way that those processes are plainly detected. By expanding the lattice region in a semilogarithm scale it is unveiled in reflectivity, Fig. 1, or in transmission, Fig. 2, well-defined first order substructure centered at around 800 cm^{-1}. In the magnetoresistive phase those extra absorption bands remain well defined, although there are significant changes in the Drude component and only at temperatures higher than 550 K does it tend to be screened by carriers (Fig. 2). The details are better seen when the continuum background is arbitrarily subtracted using a second order polynomial regression and plot, as in Fig. 3(a), in the absorption mode. They may now be recognized as a consequence of phonons interacting with the carriers—their frequencies correlating with external and internal perovskite vibrational modes.[28] Specifically, we in-

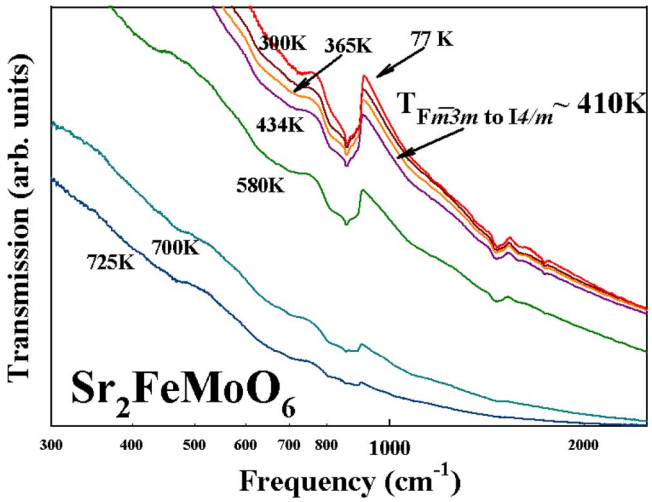

FIG. 2. (Color online) Temperature dependent transmission spectra of defect induced features in Sr_2FeMoO_6 with ~70% cationic ordering.

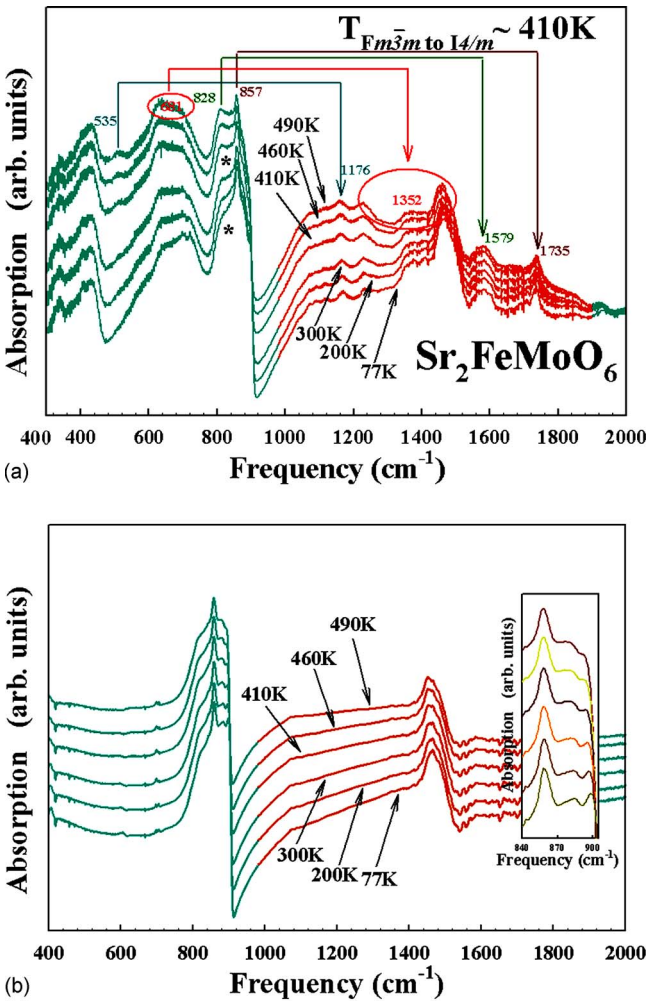

FIG. 3. (Color online) (a) First and second order absorption bands of Sr_2FeMoO_6, with ~27% Fe/Mo antisite replacements originating in strong electron-phonon interactions at frequencies near longitudinal optical modes and their respective overtones. The asterisk points to the only absorption showing the effects of octahedral tilting and rotation as reported in Ref. 8. For better viewing all spectra have been vertically displaced relative to the one at 77 K. (b) First and second order absorption bands of Sr_2FeMoO_6 with ~8% Fe/Mo antisite replacements originating in strong electron-phonon interaction at frequencies near longitudinal optical breathing modes and its overtone. For better viewing all spectra have been vertically displaced relative to the one at 77 K. The inset shows substructure denoting small octahedral distortion differences and/or oxygen defects.

terpret those bands as originating from the extra absorption due to the interaction by carriers with longitudinal optical phonons; i.e., the vibration quasipolar character proper of insulating patches, and, in particular, at the antiphase boundaries, is modified by the electrons for which long wavelength phonon screening is dynamic.[29] This effect usually reveals itself as antiresonances, punctual reductions in reflectivity on the higher frequency side of every reststrahlen band with weaker macroscopic fields. Associated with longitudinal mode softening, in our case these fields for transverse and longitudinal mode splits are totally electron screened.[30] We may then think of those features as vibrations of locally active insulating $SrFeO_{3-\delta}$-like regions originating in misplaced Fe octahedra in a rarified environment. The Fe-O-Fe configuration would be then sharing the nearest Mo electron localization with a nominally average charge $Fe^{+3.5}$ instead of Fe^{4+} found in $SrFeO_3$ (Refs. 8 and 31) with helical magnetic structure. This is also in agreement with resistivity measurements bringing up the contribution of disordered magnetic moments.[20] Defect $SrFeO_{3-\delta}$ thin films have recently been found insulating and magnetoresistive.[31] Table I shows our phonon results at 490 and 77 K in which frequencies are in reasonable agreement with those measured in $SrFeO_{3-\delta}$ thin films.[31]

It is also remarkable how easily identifiable is the second order spectrum, Fig. 3(a), establishing one more time the effects of localization in highly anharmonic Sr_2FeMoO_6. There is only one smooth and weak temperature-dependent side band, marked with an $*$ at ~858 cm^{-1} in Fig. 3(a), that gradually follows the octahedral tilting and rotation as the structural phase transition at ~410 K takes place.[8] In contrast to this, the overall spectrum does not change, supporting the idea that it ought to be associated with defects. As pointed out above, disordered Sr_2FeMoO_6 always remain in the tetragonal phase and thus phonon bands are expected to be unaltered. We then conclude that the interaction by electrons, with longitudinal optical modes inferred as first order and second order extra absorptions, provide evidence of carrier localization across the sample. In addition, it is worth noting that to have an optimum fit we need to add a broad contribution with a weak oscillator strength at frequencies where third order phonons would be found.

Figure 3(b) shows the same measurements but for a sample with only ~8% of Fe/Mo antisite disorder. In contrast with the structure found in Fig. 3(a), here, transmission spectra only illustrate the interaction of the longitudinal optical mode and its overtone. We understand this cleaner picture as a consequence of having an increase in the number of carriers and a reduction of defects that increment the phonon coherent length.

It is also worth mentioning recent resonant Raman scattering measurements in double perovskites[32] in which the Raman active symmetric stretching phonon at ~850 cm^{-1} is dominant. This and the second order spectrum[33] are concurrent in pointing to a rarefied environment (the ungerade-gerade selection rules are likely to be locally blurred) in which strong electron-phonon interactions and anharmonicities are the common denominator in double perovskites. The infrared active absorptions discussed above fall into this context.

Defects also act as barriers to electronic transport between stoichoimetric volumes where the alternating Fe by Mo order is maintained.[15] We further point to those electric dipoles detectable by infrared spectroscopy signal spin disorder by interchanged Fe/Mo crystallographic positions, thus, pointing to the destruction of the electron polarization and the overall half-metal character of our compound.[34] Either grain-point or clusters ascribe to the suppression of the spin dependent scattering at the substituting lattice defects.[18]

On the other hand, we take Tomioka *et al.*[19] single crystal null magnetoresistance detection and the absence of first and second phonon structures as additional proof that our phonon

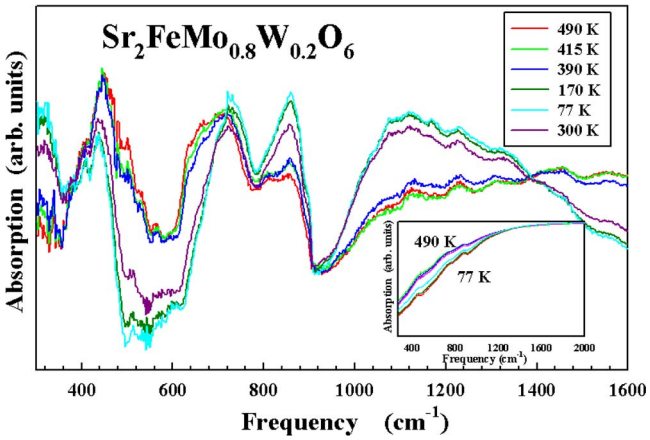

FIG. 4. (Color online) First and second order absorption bands of $Sr_2FeMo_{0.8}W_{0.2}O_6$ due to strong electron-phonon interactions at frequencies near longitudinal optical modes. Inset: temperature dependent absorption spectra of $Sr_2FeMo_{0.8}W_{0.2}O_6$.

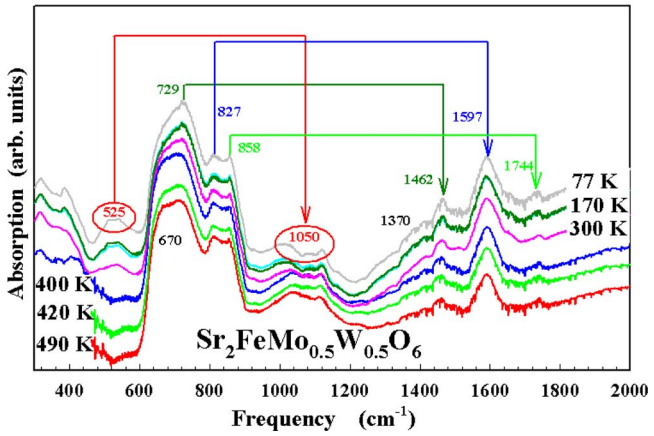

FIG. 5. (Color online) First and second order absorption bands of $Sr_2FeMo_{0.5}W_{0.5}O_6$ due to strong electron-phonon interactions at frequencies near longitudinal optical modes. For better viewing all spectra have been vertically displaced relative to the one at 490 K.

related features are associated to patches in which low-field magnetoresistance originates.[32] We also agree with Saitoh *et al.*[4] in observing that their reported anomaly ought to be reassigned. That weak bump seems to be where it should be centered, heavily averaged and screened, part of our phonon related features not noticeable in their sample because of higher carrier mobility.

Our infrared measurements support the picture that low-field magnetoresistance has an extrinsic origin but with a more intrinsic character not fundamentally requiring an intergrain mechanism. This may, however, play a role for higher values of magnetic field.[15]

V. $Sr_2FeMo_{1-x}W_xO_6$ ($x=0.2,0.5,0.8,1.0$)

In this section we report the change in the infrared spectra going from metal-like ferrimagnetic Sr_2FeMoO_6 to antiferromagnetic insulator Sr_2FeWO_6 replacing Mo by W as $x=0.20,0.50,0.80,1.0$ in the respective solid solution.

Our primary structural characterization shows that these compounds for $x=0.2,0.5$, can be described in the tetragonal $I4/m$ space group, whereas the samples with $x=0.8$ and 1 are monoclinic, space group $P2_1/n$ (Ref. 18). Besides, a decrease was observed in the number of antisite defects as the W content increases. For intermediate compositions there is a lack of translation symmetry due to random substitution at the (Mo,W) sites. Therefore, it is expected that selection rules for Raman and infrared measurements be more relaxed with the phonon coherent length depending on the local ion disorder. The increase of W content implies an increase in carrier localization. Note that in our analysis we do not consider possible Jahn-Teller effects in the lattice distortions that may further add as uncorrelated defects to the breaking of symmetry.

The spectra for $x<0.5$ are similar to the one found for the pure compound in the sense that they may be characterized as metal oxides with the resistivities behaving accordingly.[21] Figure 4 shows the temperature dependent absorption spectra for $x=0.2$. In this solid solution the main spectral feature is the secondary substructure as in the case of pure Sr_2FeMoO_6, noting, however, that the introduction of a small amount of W results in a less defined defect induced first and second order spectrum. The structural evolution of the series shows that there is an increasing amount of Fe^{2+} cations accompanying the introduction of W^{6+} cations. The difference in ion size among Fe^{2+} and Mo^{5+} and W^{6+} seems to favor cation ordering, thus increasing the phonon coherence length and the screening. Localization is detected, as the sample is cooled, in the broad band centered at ~ 1200 cm^{-1}, where an increase in absorption is noted. On it, second order bands are weakly delineated (see the below discussion for $Sr_2FeMo_{0.2}W_{0.8}O_6$).

As we further increase the amount of W, $x=0.5$, we regain the initial absorption picture now with the extra bands due to the presence of the heavier ion, for which phonon frequencies are shifted down. Figure 5 shows this for $Sr_2FeMo_{0.5}W_{0.5}O_6$, where a three component structure can be visualized, once again in the spectral region centered at 800 cm^{-1}. This now matches three octahedral breathing modes where the strongest electron-phonon interaction, and therefore the absorption, is expected, i.e., at least at patches border regions every kind of octahedra Fe, Mo, W, seems to interact individually with itinerant electrons making semiconducting clustering sources of localization for a lattice where is likely a growing population of the Fe^{2+} configuration.[11]

As a consequence, the less screened infrared active phonons from the ordered part of the lattice contributes to the spectral features precluding an independent assessment on the contribution of antisite patches as in Sr_2FeMoO_6. Nonetheless, $Sr_2FeMo_{0.5}W_{0.5}O_6$ helps to establish that the nature of our weak absorptions are vibrationally related.

Being proportional to the optical conductivity, the overall absorption spectra (Fig. 6) show the transition from *n*-type to *p*-type conductivity as a small change, presumably t_{2g} levels, in a ferrimagnetic environment at 190 K. This change is likely favored by the gradual lowering of lattice symmetry as found in previous neutron diffraction experiments[8] and the low temperature increase in the localization.

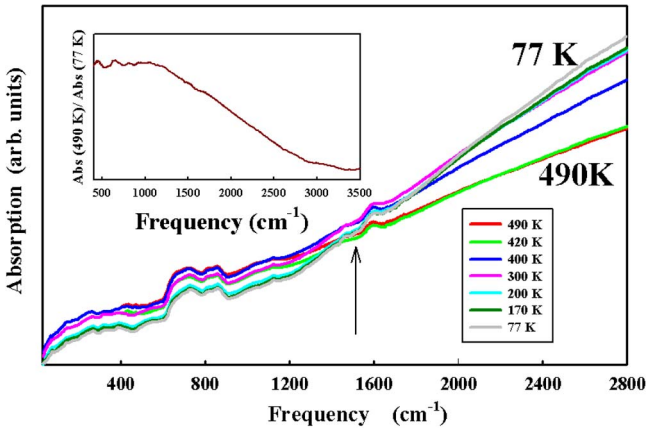

FIG. 6. (Color online) Absorption spectra of $Sr_2FeMo_{0.5}W_{0.5}O_6$. Note the change in the slope at the temperatures in which it was reported the change from *n* to *p* conductivity is also likely associated to an undergoing structural phase transition.

The insulating trend by the replacement of Mo by W is pictured for $x=0.8$ in Fig. 7. The temperature dependent reflectivity of $Sr_2FeMo_{0.2}W_{0.8}O_6$ shows spectra characteristics of an insulator in which the nearby metal to insulator transition already took place and in which now the valence W^{6+} prevails within the ion valence mixture Fe^{3+}, Fe^{2+}, W^{6+}, Mo^{6+}, and Mo^{5+} of valence fluctuating ions throughout the whole solid solution. This is the Mo/W replacement ratio for which it has been reported as the highest magnetoresistive effect.[19] The spectra are characterized by typical perovskite main vibrational bands for lattice, torsional-bending, and breathing modes at ~ 150 cm^{-1}, ~ 250 cm^{-1}, and 650 cm^{-1} respectively. There is a very weak Drude component (Fig. 7, lower left inset), yielding less than $\sim 10^{16}$ effective carriers at 77 K. As the system cools down the dielectric response shows at frequencies higher than 750 cm^{-1} an extra band centered at 900 cm^{-1} (Fig. 7, upper right inset) that it is result of localization in a small polaron picture. Note that in this case, in an effort to have a cleaner representation defined by the localization due to the 698 cm^{-1} longitudinal mode (Table II), we did not introduce in our simulation an extra weak oscillator representing second order phonon structure. Thus, the reflectivity minimum signal a very low damping constant in accordance with a very strong longitudinal optical mode-carrier interaction. This is also accompanied with softening (Ref. 29) of at least that longitudinal mode (highest frequency breathing mode) that is best seen in the semiconducting environment of $Sr_2FeMo_{0.2}W_{0.8}O_6$. This is also in agreement with having holes trapped out in an insulating matrix reported from thermoelectric power measurements[11] and is the counterpart of the situation for $x=0.0, 0.2, 0.5$ where we have a conducting matrix in which there are insulating inhomogeneous patches. There, we have phonons totally screened only revealing strong electron-phonon interac-

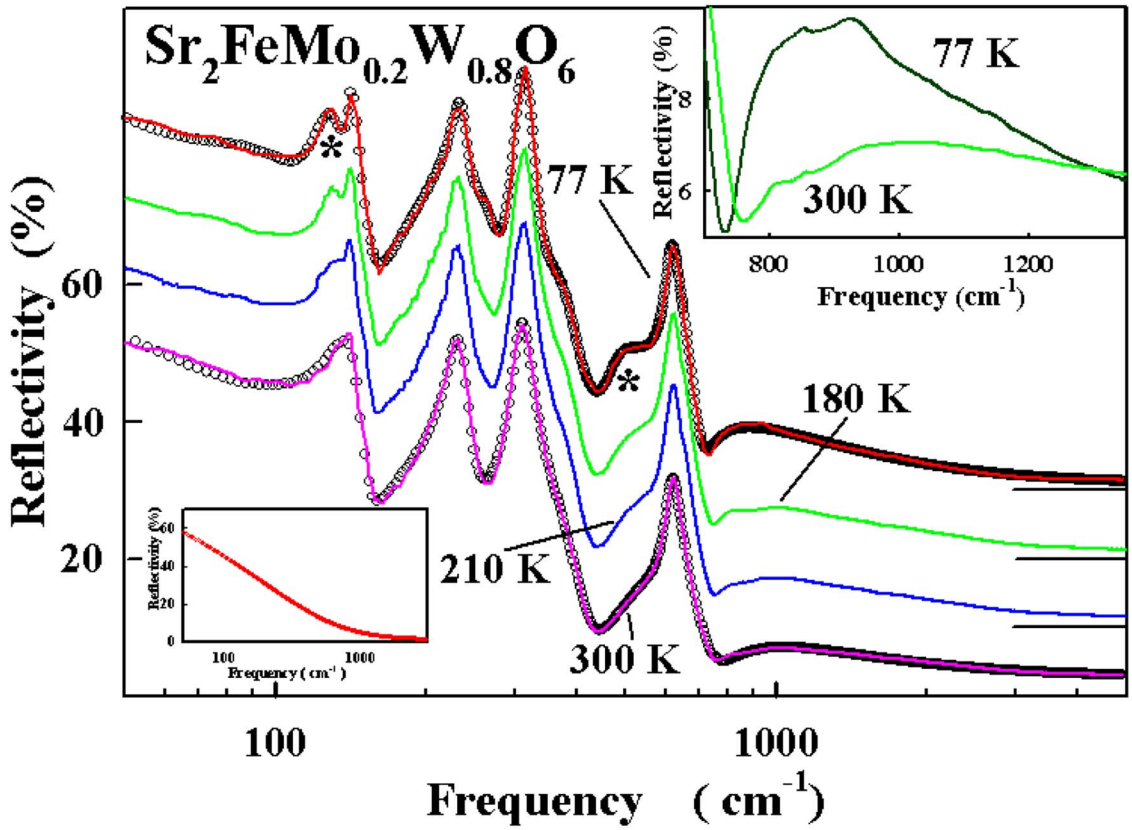

FIG. 7. (Color online) Temperature dependent reflectivity spectra of $Sr_2FeMo_{0.2}W_{0.8}O_6$. The asterisk marks new phonon activity. Full lines: experimental; open circles: fitted. For better viewing all spectra have been vertically displaced relative to the one at 300 K. Low left inset: incipient Drude component at 77 K. Upper right inset: change in reflectivity as the small polaron localization increases at 77 K. Note the minimum reflectivity redshift due to the longitudinal mode softening as the sample cools down.

TABLE II. Fitting parameters in the dielectric simulation for $Sr_2FeM_{0.2}W_{0.8}O_3$.

Temperature (K)	ε_∞	ω_{TO} (cm^{-1})	ω_{LO} (cm^{-1}) ω_p (cm^{-1})	γ_{TO} (cm^{-1}) γ_0 (cm^{-1})	γ_{LO} (cm^{-1}) γ_p (cm^{-1})	S (cm^{-2})
		101.8	109.8	100.4	41.6	2.43
		125.9	137.4	23.3	11.0	2.26
		140.4	152.0	6.6	3.4	0.37
		169.3	229.2	185.7	1229.0	1.30
		232.6	241.7	20.1	21.8	0.02
		276.2	277.4	102.8	30.5	0.02
77	1.44	303.5	342.6	25.5	38.8	0.43
		358.4	407.2	114.6	8.3	0.10
		475.1	481.3	80.4	129.8	0.02
		610.9	627.4	39.7	104.4	0.06
		692.5	698.1	141.0	4.7	0.01
			1012.7	1217.8	1055.0	
		139.1	150.9	27.0	2.5	5.28
		153.3	210.8	586.0	1175.1	0.83
		228.9	249.3	24.2	20.8	0.23
		303.9	328.9	25.6	76.5	0.45
300	1.97	353.5	410.5	227.9	10.0	0.28
		480.0	482.0	313.1	564.2	0.01
		613.9	625.8	38.4	107.8	0.07
		702.8	727.3	287.8	80.0	0.10
			723.2	854.5	870.	

tion through sharp absorptions. Here, on the contrary, phonon bands are well defined with a new band at 900 cm^{-1} for 77 K indicative of very strong charge localization in an insulting matrix. Low temperature splits of phonon bands suggests that there is a structural phase transition at the temperatures in which it is detected the change from electron to hole conductivity.[11] This process seems to be well underway in our samples at about 250 K where extra side bands are already well defined. Figure 8 shows transverse optical modes as maxima of the optical conductivity at 77 K where

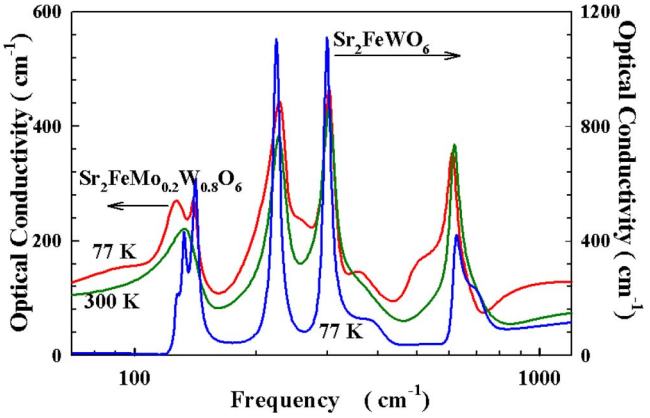

FIG. 8. (Color online) Optical conductivity of $Sr_2FeMo_{0.2}W_{0.8}O_6$ at 300 and 77 K. The better defined narrower peaks due to the optical conductivity of Sr_2FeWO_6 at 77 K are shown on the right vertical axis (after Ref. 36).

it has also contrasted their definition against for those active in Sr_2FeWO_6.

As we have already reported,[36] infrared reflectivity shows that Sr_2FeWO_6 is an antiferromagnetic ($T_N \sim 37$ K) insulator structurally stable from 77 to 700 K with a gap about 750 cm^{-1} ($\sim$95 meV) and with Fe^{2+} in the high spin state ($S=2$) (Ref. 32) and W^{6+} ($5d^0$) in a nonmagnetic state.[35] The optical conductivity suggests that lattice arrangement for the lower temperature for $x=0.8$ seems to be driven by the monoclinic $P2_1/n$ space group of the W pure end compound.[36]

Overall, we reason that our results for the $Sr_2FeMo_{1-x}W_xO_6$ ($x=0.20, 0.50, 0.80, 1.0$); solid solutions fall into the prevailing approach for doped manganites. In these compounds there is coexistence of conducting and insulating regions that would yield a double-exchange like metal-oxide fraction contiguous to more insulating regions in which a lattice polaron localization would prevail.[37,38] Modeling mixed phase resistivity also yields negative magnetoresistance in the vicinity of a Curie temperature.[39] And as in manganites, where it is known that localized carriers continue to exist in the metallic phase, the regions of self-trapped strong localizations are identified as those related to electron-phonon interactions in which the phonon involved corresponds to the longitudinal optical mode of every reststrahlen band, being the strongest for breathing modes at the highest vibrational frequencies.

Summarizing, the infrared reflectivity of Sr_2FeMoO_6 with about 27% of antisite defects reveal phonon related substruc-

tures on the metal oxide Drude component. Their origin may be traced to extra absorptions due to the interaction of longitudinal optical modes with carriers in a semiconducting environment related to Fe, Mo, W patches in a crystallographic lattice.

The comparison between the transmission spectra of samples of Sr_2FeMoO_6 with ~70% and ~92% of Fe/Mo cationic ordering shows that by reducing the number of defects there is an increment in the phonon coherent length yielding a cleaner picture in the most perfectly ordered sample.

We argue that it is at a nanoscale where those interacting carriers, their confinement, particularly at the border regions, antiphase boundaries, and the important polaronic effects, will yield the main clue for understanding electron localization and thus low-field magnetoresistance. They become more mobile under moderate magnetic fields yielding a more intrinsic character to magnetoresistive effects. Then, as found in Mössbauer spectroscopy,[12] when a magnetic field is applied to this region on either side of patches boundaries, carriers are aligned but there is also a quasidomain wall at the boundary which narrows, thinning the electronic barriers due to a reduction of the electron-phonon interaction. The effect is reminiscent to the magnetic field induced insulator-metal transition as observed in manganites where a crossover to a metal-oxide conductor from an insulating state is observed upon the application of a magnetic field., i.e., metamagnetic transitions where even charge-order melts.[40] The low-field magnetoresistance is enhanced with increasing field.

We conclude that moderate antisite disorder plays a significant role in explaining low-field magnetoresistance adding to the always present contribution to connectivity and lattice defects distributed at random in the sample. On the other hand, larger patched regions may preclude the electronic transport.[41] Then, quantitatively exploiting this fact with techniques generating controlled defective environments we might find imperfect compounds having the adequate magnetoresistance at low fields and ambient temperature for practical applications. As it was pointed out earlier, low-field magnetoresistance depends monotonically on the presence of those imperfections.[15]

ACKNOWLEDGMENTS

J. A. A., M. J. M-L, and M. T. C. acknowledge the financial assistance of the Ministerio de Ciencia y Tecnología (Spain) under Project No. MAT2004-0479.

*Email address: nem@dalton.quimica.unlp.edu.ar

[1] S. Nakayama, T. Nakagawa, and S. Nomura, J. Phys. Soc. Jpn. **24**, 219 (1968).
[2] J. Longo and R. Word, J. Am. Chem. Soc. **83**, 2816 (1961).
[3] F. K. Patterson, C. W. Moeller, and R. Word, Inorg. Chem. **2**, 196 (1963).
[4] T. Saitoh, M. Nakatake, A. Kakizaki, H. Nakajima, O. Morimoto, Sh. Xu, Y. Moritomo, H. Hamada, and Y. Aiura, Phys. Rev. B **66**, 035112 (2002).
[5] D. D. Sarma, Prya Mahadevan, T. Saha-Dasgupta, Sugata Ray, and Ashwani Kumar, Phys. Rev. Lett. **85**, 2549 (2000).
[6] Z. Fang, K. Terakura, and J. Kanamori, Phys. Rev. B **63**, 180407(R) (2001).
[7] K.-I. Kobayasi, T. Kimura, H. Sawada, K. Terakura, and Y. Tokura, Nature (London) **395**, 677 (1998).
[8] D. Sánchez, J. A. Alonso, M. García-Hernández, M. J. Martínez-Lope, J. L. Martínez, and A. Mellergard, Phys. Rev. B **65**, 104426 (2002).
[9] D. Niebieskikwiat, R. D. Sánchez, A. Caneiro, L. Morales, M. Vásquez-Mansilla, F. Rivadulla, and L. E. Hueso, Phys. Rev. B **62**, 3340 (2000).
[10] M. Tovar, M. T. Causa, A. Butera, J. Navarro, B. Martínez, J. Foncuberta, and M. C. G. Passeggi, Phys. Rev. B **66**, 024409 (2002).
[11] J. M. Greneche, M. Venkatesan, R. Suryanarayanan, and J. M. D. Coey, Phys. Rev. B **63**, 174403 (2001).
[12] J. Lindén, T. Yamamoto, M. Karppinen, and H. Yamauchi, Appl. Phys. Lett. **76**, 2925 (2000).
[13] R. I. Dass and J. B. Goodenough, Phys. Rev. B **63**, 064417 (2001).
[14] M. Karppinen, H. Yamauchi, Y. Yasukawa, J. Lindén, T. S. Chan, R. S. Liu, and J. M. Chen, Chem. Mater. **15**, 4118 (2003).
[15] M. García-Hernández, J. L. Martínez, M. J. Martínez-Lope, M. T. Casais, and J. A. Alonso, Phys. Rev. Lett. **86**, 2443 (2001).
[16] M. Retuerto, J. A. Alonso, M. J. Martínez-Lope, J. L. Martínez, and M. García-Hernández, Appl. Phys. Lett. **85**, 266 (2004).
[17] N. E. Massa, H. Falcón, H. Salva, and R. E. Carbonio, Phys. Rev. B **56**, 10 178 (1997).
[18] D. Sánchez, J. A. Alonso, M. García-Hernández, M. J. Martínez-Lope, and M. T. Casais, J. Phys.: Condens. Matter **17**, 3673 (2005).
[19] Y. Tomioka, T. Okuda, Y. Okimoto, R. Kumai, K.-I. Kobayashi, and Y. Tokura, Phys. Rev. B **61**, 422 (2000).
[20] H. Yanagihara, M. B. Salamon, Y. Lyanda-Geller, Sh. Xu, and Y. Moritomo, Phys. Rev. B **64**, 214407 (2000).
[21] O. Chmaissem, R. Kruk, B. Dabrowski, D. E. Brown, X. Xiong, S. Kolesnik, J. D. Jorgensen, and C. W. Kimball, Phys. Rev. B **62**, 14 197 (2000).
[22] K.-I. Kobayashi, T. Okuda, Y. Tomioka, T. Kimura, and Y. Tokura, J. Magn. Magn. Mater. **218**, 17 (2000).
[23] T. Kurosawa, J. Phys. Soc. Jpn. **16**, 1208 (1961).
[24] F. Gervais, J. L. Servoin, A. Baratoff, J. B. Berdnorz, and G. Binnig, Phys. Rev. B **47**, 8187 (1993).
[25] Y. Moritomo, Sh. Xu, A. Machida, T. Akimoto, E. Nishibori, M. Takata, and M. Sakata, Phys. Rev. B **61**, R7827 (2000).
[26] J. H. Jung, S.-J. Oh, M. W. Kim, T. W. Noh, J.-Y. Kim, J.-H. Park, H.-J. Lin, C. T. Chen, and Y. Moritomo, Phys. Rev. B **66**, 104415 (2002).
[27] R. Muehlstroh and H. G. Reik, Phys. Rev. **162**, 703 (1967).
[28] M. Couzi and P. V. Huong, J. Chim. Phys. **69**, 1339 (1972).
[29] M. Reizer, Phys. Rev. B **61**, 40 (2000).
[30] L. A. Faskovsky, Phys. Rev. B **66**, 020302(R) (2002).

[31] Lebon, P. Adler, C. Bernhard, A. V. Boris, A. V. Pimenov, A. Maljuk, C. T. Lin, C. Ulrich, and B. Keimer, Phys. Rev. Lett. **92**, 037202 (2004).

[32] J. Andreasson, J. Holmlund, L. Brjesson, and M. Kll, Bull. Am. Phys. Soc. **49**(1), 293 (2004); J. Andreasson, J. Holmlund, K. Käll, S. Naler, J. BÄckström, M. Rübhausen, A. K. Azad, and S.-G. Eriksson, *ibid.* **50**, 542 (2005).

[33] J. Andreasson, Lic. thesis, University of Technology, Sweden, 2005.

[34] See also, R. Panguluri, B. Nadgorny, X. Dheng, and Y. Moritono, Bull. Am. Phys. Soc. **48**, 603 (2003).

[35] II. Q. Yin, J. S. Zhou, R. Dass, J. P. Zhou, J. T. McDevitt, and J. B. Goodenough, Appl. Phys. Lett. **75**, 2812 (1999); J. Appl. Phys. **87**, 6761 (2000).

[36] F. P. de la Cruz, N. E. Massa, J. A. Alonso, M. J. Martínez-Lope, and M. T. Casais, Solid State Commun. **127**, 703 (2003).

[37] H. Kawanaka, I. Hase, S. Toyama, and Y. Nishihara, Physica B **284**, 1428 (2000); **281–282**, 518 (2000).

[38] H. Kawanaka, I. Hase, S. Toyama, and Y. Nishihara, J. Phys. Soc. Jpn. **68**, 2890 (1999).

[39] A. Weiβe, J. Loos, and H. Fehske, Phys. Rev. B **68**, 024402 (2003), and references therein.

[40] V. Hardy, A. Wahl, C. Martin, and Ch. Simon, Phys. Rev. B **63**, 224403 (2001).

[41] See also, D. Niebieskikwiat, F. Prado, A. Caneiro, and R. D. Sánchez, Phys. Rev. B **70**, 132412 (2004).